Supplementary Information (*SI Appendix*)

Wireless, Soft Electronics for Rapid, Multi-sensor Measurements of Hydration Levels in Healthy and Diseased Skin.

Kyeongha Kwon[a,b,1], Heling Wang[c,d,e,1], Jaeman Lim[a,f], Keum San Chun[g], Hokyung Jang[h], Injae Yoo[b], Derek Wu[a,e], Alyssa Jie Chen[a], Carol Ge Gu[a], Lindsay Lipschultz[i], Jong Uk Kim[j], Jihye Kim[a,k] Hyoyoung Jeong[a], Haiwen Luan[a, c,d,e], Yoonseok Park[a], Chun-Ju Su[a], Yui Ishida[l], Surabhi R. Madhvapathy[a, d], Akihiko Ikoma[l], Jean Won Kwak[a, e], Da Som Yang[a], Anthony Banks[a], Shuai Xu[a,i,m], Yonggang Huang[c,d,e], Jan-Kai Chang[a,f,2], John A. Rogers[a, d,e,i,n,2]

[a]Querrey-Simpson Institute for Bioelectronics, Northwestern University, Evanston, IL, USA.

[b]School of Electrical Engineering, Korea Advanced Institute of Science and Technology, Daejeon, Republic of Korea.

[c]Department of Civil and Environmental Engineering, Materials Science and Engineering, Northwestern University, Evanston, IL, USA.

[d]Department of Materials Science and Engineering, Northwestern University, Evanston, IL, USA.

[e]Department of Mechanical Engineering, Northwestern University, Evanston, IL, USA.

[f]Wearifi Inc., Evanston, IL, USA.

[g]Electrical and Computer Engineering, the University of Texas at Austin, Austin, TX, USA.

[h]Department of Electrical & Computer Engineering, University of Wisconsin, Madison, WI, USA.

[i]Department of Biomedical Engineering, Northwestern University, Evanston, IL, USA.

[j]School of Chemical Engineering, Sungkyunkwan University, Suwon, Republic of Korea.

[k]School of Advanced Materials Science and Engineering, Sungkyunkwan University, Suwon, Republic of Korea.

[l]Maruho Co., Ltd., Osaka, Japan.

[m]Department of Dermatology, Feinberg School of Medicine, Northwestern University, Chicago, IL, USA.

[n]Departments of Neurological Surgery, Chemistry, Chemical Engineering, Electrical Engineering and Computer Science; Northwestern University, Evanston, IL, USA.

[1]K.K. and H.W. contributed equally to this work.

[2]To whom correspondence may be addressed. E-mail: jrogers@northwestern.edu, or jkchang@mywearifi.com.

Keywords: wireless electronics, flexible electronics, bioelectronics, biomedical devices, skin, diagnostics, health monitoring, sensors.

Supplementary Information

Supplementary Figure S1-S19

Supplementary Table S1-S5

Supplementary Text ST1-ST3

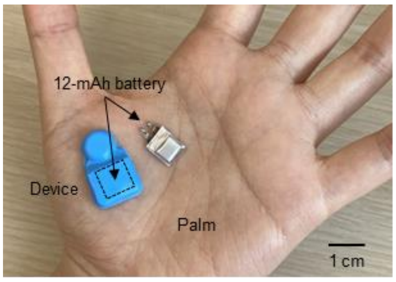

Figure S1. Picture of an encapsulated device next to a 12 mAh Li-polymer battery.

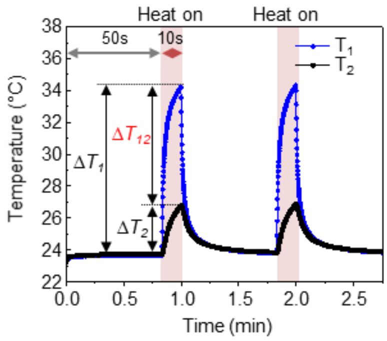

Figure S2. Wireless read-out of the temperature change measured from NTC_1 (ΔT_1) and NTC_2 (ΔT_2) as a function of time for 10 s of heating every one min. $\Delta T_{12} = \Delta T_1 - \Delta T_2$.

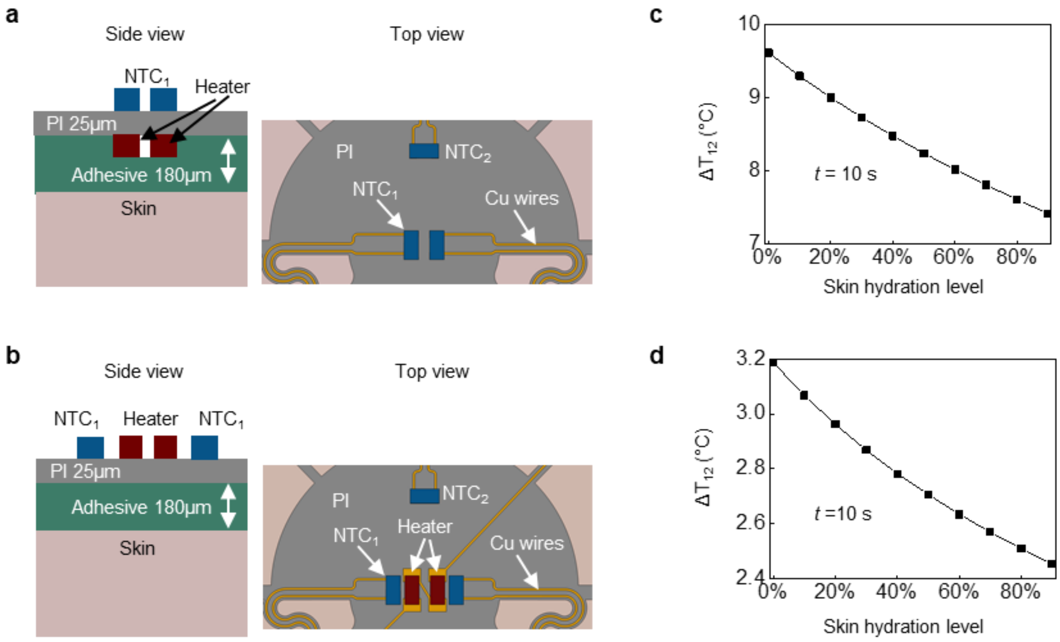

Figure S3. a,b. Schematic illustration of the FEA model of dual-sided (**a**) and single-sided (**b**) sensor designs. **c,d.** Sensitivities of the temperature difference (ΔT_{12}) between NTC_1 (ΔT_1) and NTC_2 (ΔT_2) to skin hydration level of dual-sided (**c**) and single-sided (**d**) designs 10 s after the heater is activated.

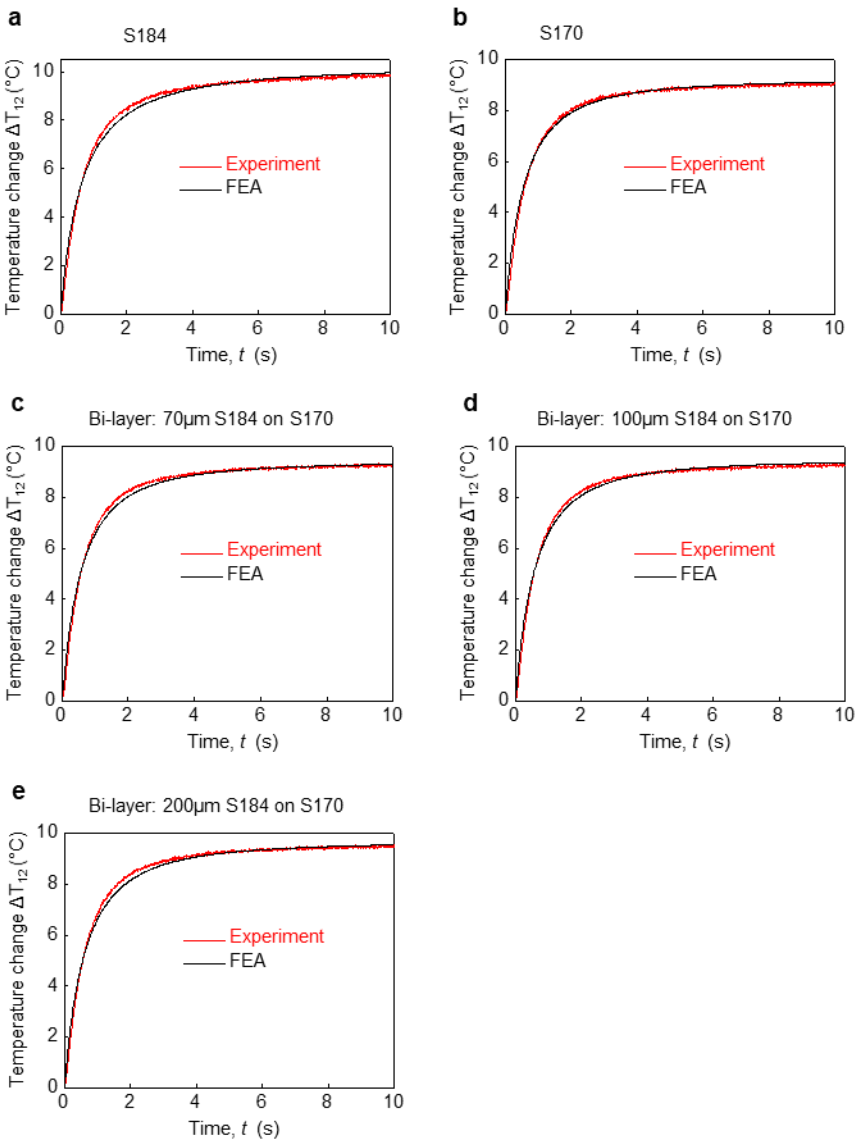

Figure S4. Comparison between FEA and measurement for a thick layer of S184 (**a**) and S170 (**b**), and a thin layer of S184 (70 µm, **c**; 100 µm, **d**; 200 µm, **e**) on top of the S170.

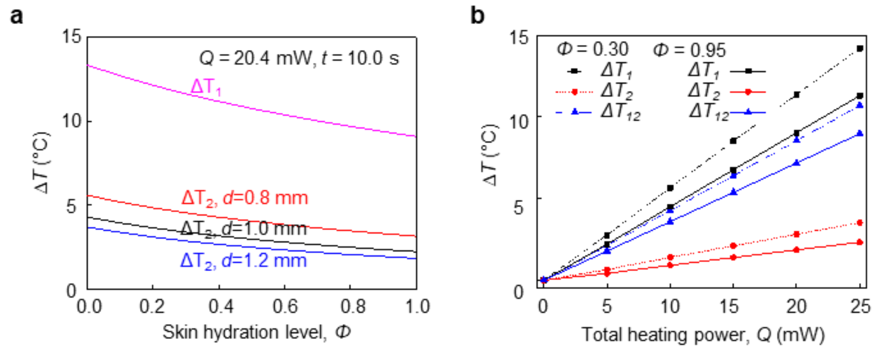

Figure S5. Computational predictions of ΔT as a function of skin hydration level (Φ) with different values of d (**a;** Q = 20.4 mW, t = 10.0 s), and ΔT as a function of Q (**b**; d = 1.2 mm, t = 10.0 s).

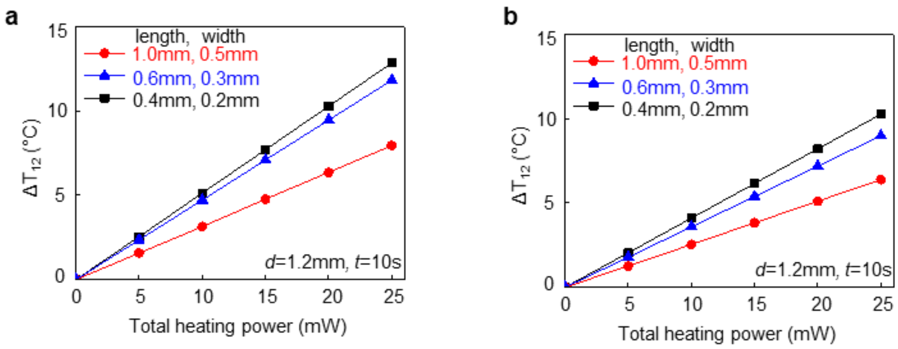

Figure S6. Computational prediction of ΔT_{12} with different sizes of actuators (width and length of R_H) for 30 % (**a**) and 95 % (**b**) hydrated skin.

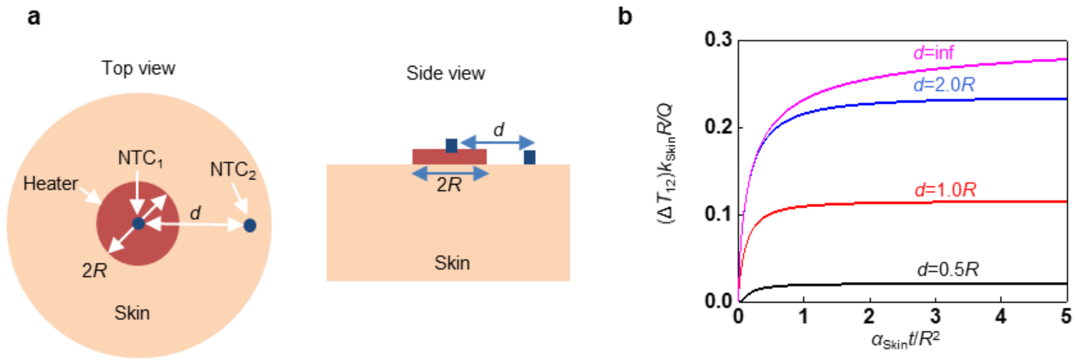

Figure S7. Effect of design parameters on the temperature change. a. A simplified, analytical model of a disk-shaped thermal actuator (radius, R) and NTCs. **b**. Analytical scaling law for ΔT_{12}

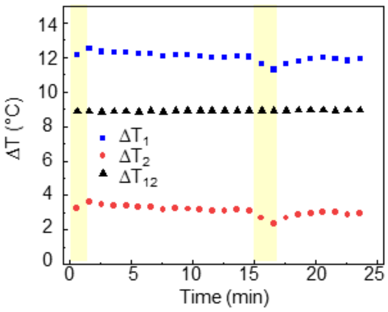

Figure S8. Ambient temperatures. Measurements of ΔT_1 (blue), ΔT_2 (red), and ΔT_{12} (black) as a function of time (min). The values of ΔT_1 and ΔT_2 fluctuate at the moment the device enters and exits the oven (yellow background).

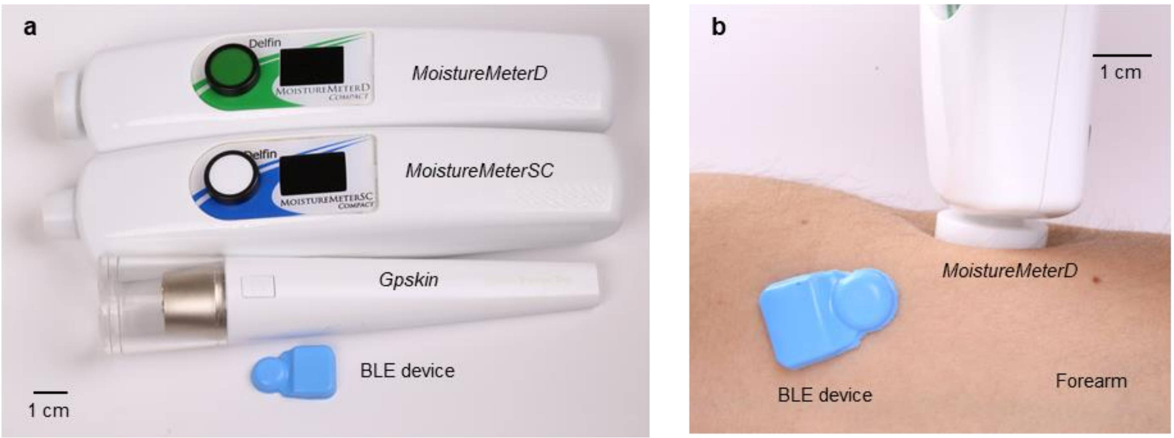

Figure S9. a. Picture of conventional devices based on skin capacitance measurements for monitoring tissue water content (*MoistureMeterD*; top), SC hydration levels (*MoistureMeterSC*; middle top), and skin surface hydration levels (*Gpskin*; middle bottom), and a BLE device (bottom). **b**. Picture of devices on the forearm. The commercial devices require care by the user to hold the probe and apply a certain pressure against the skin for each measurement.

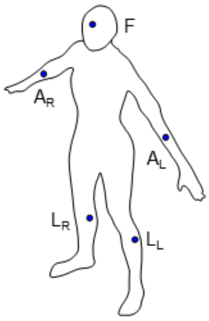

Figure S10. Mounting positions on the body: forehead (F), right arm (A_R), left arm (A_L), right leg (L_R), and left leg (L_L).

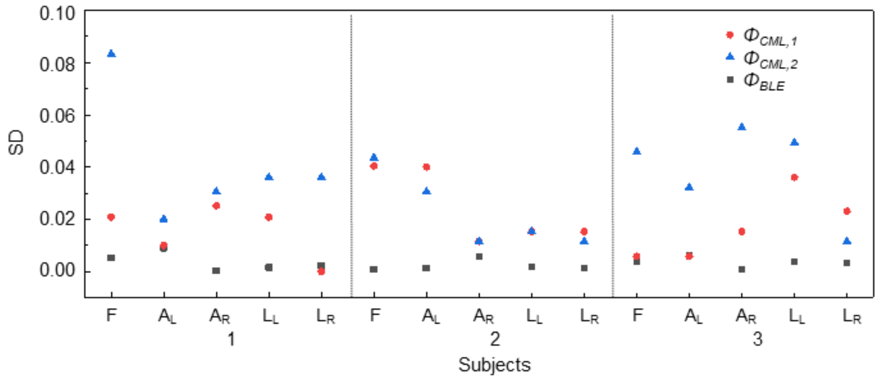

Figure S11. SD for Φ tested by 3 users using BLE (Φ_{BLE}) and commercial ($\Phi_{CML,1}$and $\Phi_{CML,2}$) devices at five different body locations, forehead (F), right arm (A_R), left arm (A_L), right leg (L_R), and left leg (L_L), for subject 1 to 3.

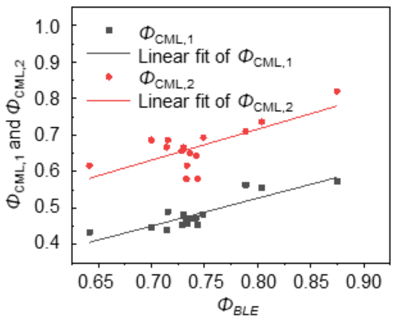

Figure S12. Positive correlation between Φ_{BLE} and $\Phi_{CML,1}$ (black), and between Φ_{BLE} and $\Phi_{CML,2}$ (red), and their linear fits (lines).

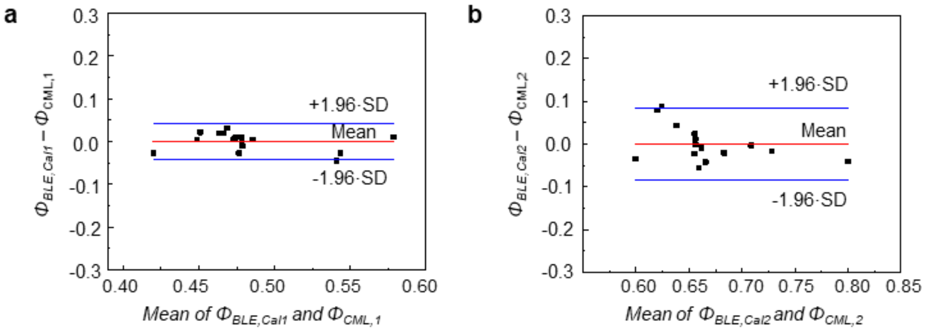

Figure S13. Bland-Altman plots of $\Phi_{BLE,Cal1}$ and $\Phi_{CML,1}$ (**a**), and $\Phi_{BLE,Cal2}$ and $\Phi_{CML,2}$ (**b**). Horizontal lines represent the mean (red), and mean±1.96·SD (blue) values of $\Phi_{BLE,Cal} - \Phi_{\mathrm{CML}}$ where SD is the standard deviation. The mean±SD values of the differences ($\Phi_{\mathrm{CML,1}} - \Phi_{\mathrm{BLE,Cal1}}$, and $\Phi_{\mathrm{CML,2}} - \Phi_{\mathrm{BLE,Cal2}}$) are 0.00±0.02 and 0.00±0.04, respectively.

Figure S14. Pictures of an encapsulated device mounted on a pediatric hand.

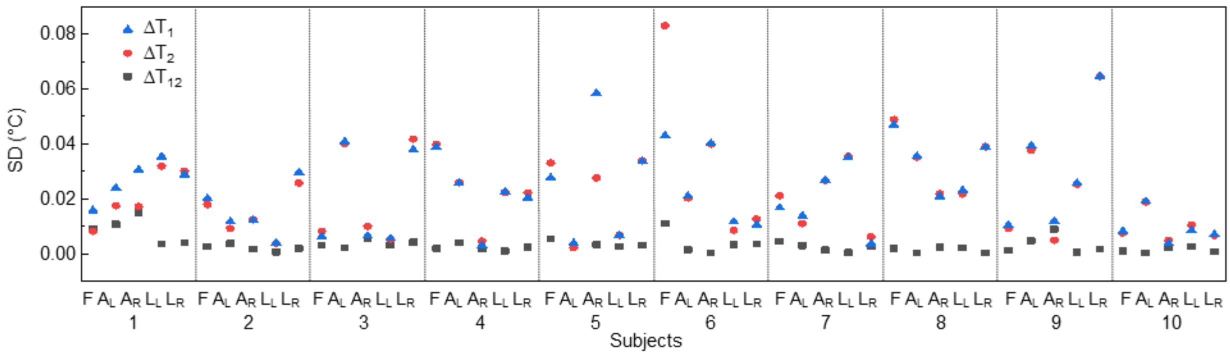

Figure S15. SD for ΔT_1, ΔT_2, and ΔT_{12} at five different body locations, forehead (F), right arm (A_R), left arm (A_L), right leg (L_R), and left leg (L_L), for subjects 1 to 10

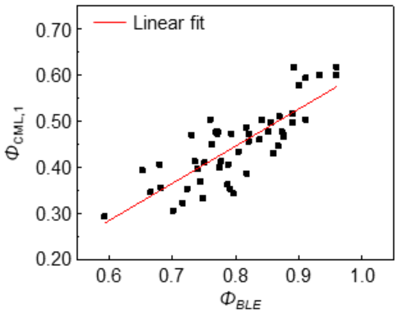

Figure S16. Positive correlation between skin hydration level from wireless (Φ_{BLE}) and commercial ($\Phi_{CML,1}$) devices, and its linear fit (red line). Linear fits indicate that $\Phi_{\mathrm{CML,1}} = \Phi_{\mathrm{BLE}} \times 0.80 - 0.20$, with a coefficient of determination of $R^2 = 0.66$.

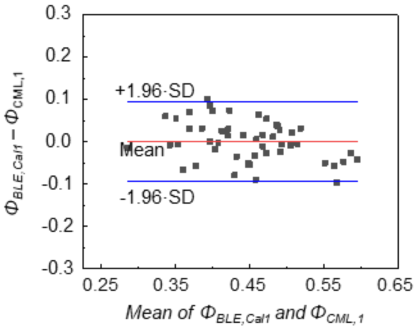

Figure S17. A Bland-Altman plot (difference plot) of $\Phi_{BLE,Cal1}$ and $\Phi_{CML,1}$. Horizontal lines represent the mean (red; ~0.00), and mean±1.96·SD (blue; ~0.00±1.96·0.05) values of $\Phi_{BLE,Cal1} - \Phi_{\mathrm{CML},1}$ where SD is the standard deviation.

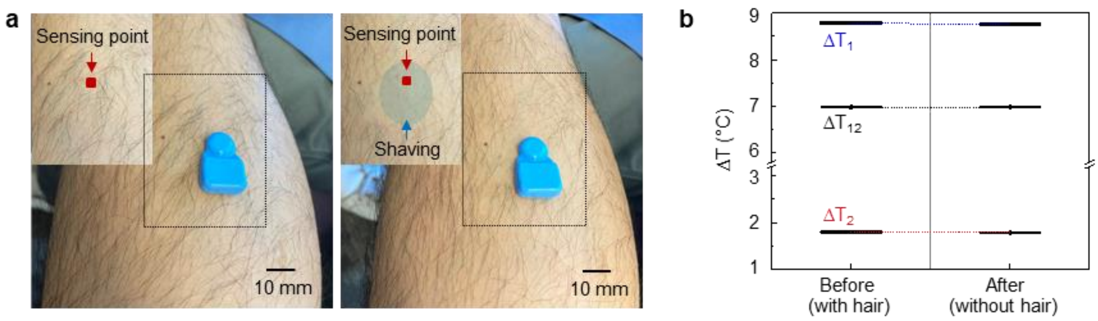

Figure S18. a. Pictures of the device on a subject's leg before (left) and after (right) shaving the skin. Insets show the sensing point. **b.** Wireless measurements of ΔT_1 (blue), ΔT_2 (red), and ΔT_{12} (black) before and after shaving the sensing area.

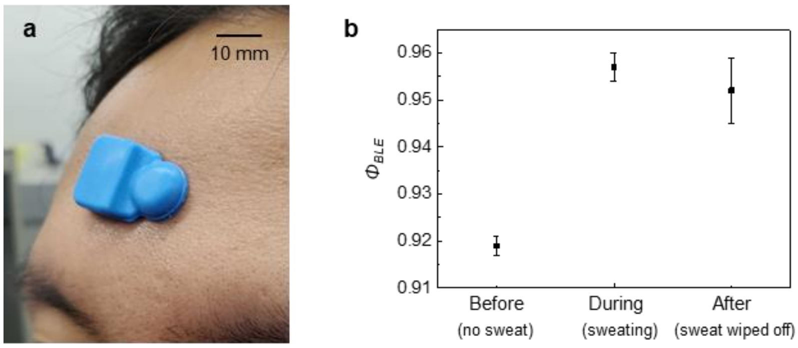

Figure S19. a. An optical image of the device mounted on the forehead of a healthy male subject. **b.** Wireless measurements of Φ_{BLE} before, during and after a workout. Vertical bar denotes the error bar over 3-time measurements.

Figure S20. Optical image of the device mounted on the atopic hand of a subject 1, next to a BLE-enabled smartphone.

Time (min)	0-10	10-30	30-35	35-45	45-81	85-91
	Abrupt change in T_S		Airflow			Airflow
SNR (dB) of ΔT_1	33	43	33	44	44	41
SNR (dB) of ΔT_2	22	32	20	32	34	30
SNR (dB) ΔT_{12}	**58**	**59**	**66**	**61**	**54**	**66**

Table S1. Signal-to-noise ratio (SNR) with different temperatures of the testing substrate (T_S) for natural air convection and for forced air flow at rates of 0~13.6 m/s from the top.

Subject number	Age	Sex	Ethnicity	Fitzpatrick Skin Type
1	25	F	Caucasian	I
2	26	F	Asian	II
3	27	M	Asian	II
4	29	M	Asian	II
5	36	M	Caucasian	I
6	16	M	Caucasian	I
7	17	M	Caucasian/Asian	I
8	24	M	Caucasian	I
9	27	F	Asian	II
10	33	M	Asian	II

Table S2. Information of the 10 healthy normal subjects.

Subject number	Age	Sex	Ethnicity	Pathology
1	22	Female	African American	AD
2	69	Male	Latinx	AD

Table S3. Information of the patients who participated in the moisturizer study

		BLE		*MoistureMeterD*		*Gpskin*			
		$\Phi_{BLE,Cal}$		$\Phi_{CML,1}$		$\Phi_{CML,2}$		TEWL	SCH
		mean	SD	Mean	SD	mean	SD		
AD	**before**	0.17	0.00	0.24	0.03	0.50	0.00	17	0
	after	0.32	0.00	0.36	0.01	0.91	0.01	33	41
Control	**before**	0.38	0.00	0.36	0.01	0.55	0.02	6	5
	after	0.46	0.00	0.44	0.01	0.96	0.02	21	46

Table S4. Φ measurements of a young adult patient with severe AD (subject 1).

		BLE		MoistureMeterD		Gpskin			
		$\Phi_{BLE,Cal}$		$\Phi_{CML,1}$		$\Phi_{CML,2}$		TEWL	SCH
		mean	SD	mean	SD	mean	SD		
Inflamed	**Before**	0.29	0.00	0.31	0.03	0.55	0.02	22	5
	After	0.46	0.00	0.44	0.01	1.00	0.00	19	53
Perilesional	**Before**	0.45	0.01	0.43	0.01	0.85	0.03	6	35
	After	0.47	0.00	0.49	0.01	0.98	0.01	4	48
Control	**Before**	0.49	0.00	0.44	0.01	0.79	0.05	5	29
	After	0.49	0.00	0.51	0.01	0.95	0.02	2	45

Table S5. Φ measurements of an elderly patient with inflammatory AD (subject 2).

Text ST1. Macroscale modeling by finite element analysis (FEA).

At the macroscale, FEA establishes a relationship between ΔT_{12} and the thermal conductivity and thermal diffusivity of the epidermis and dermis (k_E, α_E, k_D and α_D) based on the transient heat transfer analysis using the software ABAQUS. A schematic illustration of the FEA model is given in Supplementary Fig. 3a. A refined mesh (~1 million elements) with mesh size much smaller than the finest feature size of the device (18 μm, copper thickness) and a refined time increment that limits the maximum temperature change to below 0.5 °C in each increment ensure the simulation convergence and accuracy. The literature values of the material parameters are k_{copper}=377 W/(m-K), α_{copper}=109 mm^2/s, k_{PI}=0.55 W/(m-K), α_{PI}=0.32 mm^2/s, k_{Ecoflex}=0.21 W/(m-K), $\alpha_{\mathrm{Ecoflex}}$=0.11 mm^2/s.[S1] The thermal conductivity of polyimide (PI) is determined as k_{PI}=0.55 W·m^{-1}·K^{-1} from the measurements on a material with known thermal properties (S170, k_{S170}=0.40 W·m^{-1}·K^{-1}, α_{S170} =0.14 mm^2·s^{-1} [S2, S3]). For validation, a different material (S184) with known thermal properties (k_{S184}=0.20 W·m^{-1}·K^{-1}, α_{S184} =0.11 mm^2·s^{-1} [S2, S3]) and the bi-layer material of thin S184 (70~200 μm thickness) on thick S170 are tested, and the FEA results agree well with experiments without any additional fitting (Supplementary Fig. 4).

Text ST2. Micromechanics model for the thermal properties of hydrated skin.

A micromechanics model establishes a relationship between the thermal properties of hydrated skin and its hydration level Φ (volumetric water content). The hydrated skin is modeled as a composite of dry skin (thermal conductivity k_{dry} = 0.2 W·m^{-1}·K^{-1}, thermal diffusivity α_{dry} = 0.15 mm^2·s^{-1}) and water (k_{W} = 0.6 W·m^{-1}·K^{-1}, α_{W} = 0.14 mm^2·s^{-1}) [S2, S3], which gives the thermal conductivity k_{skin} and thermal diffusivity α_{skin} of the hydrated skin as

$$\frac{k_{\text{skin}}}{k_{\text{dry}}}=\frac{(p+2)+2(p-1)\Phi}{(p+2)-(p-1)\Phi},\ p=\frac{k_{\text{W}}}{k_{\text{dry}}},$$

$$\frac{\alpha_{\text{skin}}}{\alpha_{\text{dry}}}=\frac{\alpha_{\text{W}}k_{\text{skin}}}{(1-\Phi)\alpha_{\text{W}}k_{\text{dry}}+\Phi\alpha_{\text{dry}}k_{\text{W}}},$$

respectively.

For the bi-layer model of the epidermis and dermis layers for the skin, the above micromechanics model applies to each layer, with the subscript 'skin' replaced by 'E' and 'D' for epidermis and dermis, respectively.

Text ST3: A simplified analytical model.

A simplified model for the relationship between the NTC_1-to-NTC_2 spacing and their temperature difference is useful. The data in Supplementary Fig. 5 correspond to FEA results for ΔT (Q = 20.4 mW, t = 10 s) as a function of Φ with different distances (d) between NTC_1 and NTC_2, and ΔT as a function of Q (t = 10 s, d = 1.2 mm, $\Phi = 0.3$). The value of ΔT_{12} increases as d and Q increase, and as Φ decreases. The effect of actuator size (width and length of R_H) on ΔT_{12} is in Supplementary Fig. 6. As shown in Supplementary Fig. 7a, a disk-shaped heater (radius R and heating power Q) and two infinitesimal sensors rest on a semi-infinite, homogenous substrate with the properties of skin (thermal conductivity k_{skin} and thermal diffusivity α_{skin}). The heater and sensors have negligible thicknesses. The position of NTC_1 is directly above the heater (r=0 in the polar coordinate system) and NTC_2 is at a distance d from NTC_1. The temperature changes[S3] in NTC_1 and NTC_2 are

$$\Delta T_1=\frac{Q}{\pi R k_{\text{skin}}}\int_0^{+\infty}\left[J_1(x)\,erfc\left(-x\sqrt{\frac{t\alpha_{\text{skin}}}{R^2}}\right)\right]\frac{\mathrm{d}x}{x},$$

$$\Delta T_2 = \frac{Q}{\pi R k_{\text{skin}}} \int_0^{+\infty} \left[J_0\left(\frac{xd}{R}\right) J_1(x)\, erfc\left(-x\sqrt{\frac{t\alpha_{\text{skin}}}{R^2}}\right) \right] \frac{\mathrm{d}x}{x},$$

respectively, where $J_0(x)$ and $J_1(x)$ are Bessel functions of the first kind with zero- and first-orders, respectively, and $erfc(x)$ is the complementary error function. Therefore, the temperature difference between the two sensors can be expressed in the following dimensionless form

$$\frac{(\Delta T_1 - \Delta T_2) R k_{\text{skin}}}{Q} = \frac{1}{\pi} f\left(\frac{t\alpha_{\text{skin}}}{R^2}, \frac{d}{R}\right).$$

The function f is plotted in Supplementary Fig. 7b. The measurement sensitivity increases with $\frac{t\alpha_{\text{skin}}}{R^2}$ or $\frac{d}{R}$.

References

[S1] K. E. Crawford et al., Advanced approaches for quantitative characterization of thermal transport properties in soft materials using thin, conformable resistive sensors. Extreme Mech. Lett. **22**, 27–35 (2018).

[S2] Madhvapathy, S. R. *et al.* Reliable, Low-Cost, Fully Integrated Hydration Sensors for Monitoring and Diagnosis of Inflammatory Skin Diseases in Any Environment. Under review.

[S3] Madhvapathy, S. R. *et al.* Epidermal Thermal Depth Sensors: Epidermal Electronic Systems for Measuring the Thermal Properties of Human Skin at Depths of up to Several Millimeters. *Adv. Funct. Mater.* **28**, 1870242 (2018).

[S4] S. Krishnan et al., Multimodal epidermal devices for hydration monitoring. *Microsystems & Nanoengineering* **3**, 17014 (2017).

[S5] E. Behrens, Thermal Conductivities of Composite Materials. J. Compos. Mater. **2**, 2–17 (1968).